Journal of Power Sources 196 (2011) 4174–4180

Contents lists available at ScienceDirect

Journal of Power Sources

journal homepage: www.elsevier.com/locate/jpowsour

Synthesis of highly ordered three-dimensional nanostructures and the influence of the temperature on their application as solid oxide fuel cells cathodes

R. Pinedo[a], I. Ruiz de Larramendi[a], D. Jimenez de Aberasturi[a], I. Gil de Muro[a], J.I. Ruiz de Larramendi[a], M.I. Arriortua[b], T. Rojo[a,*]

[a] Departamento de Química Inorgánica, Facultad de Ciencia y Tecnología, Universidad del País Vasco UPV/EHU, Apdo. 644, 48080 Bilbao, Spain
[b] Departamento de Mineralogía y Petrología, Facultad de Ciencia y Tecnología, Universidad del País Vasco UPV/EHU, Apdo. 644, 48080 Bilbao, Spain

ARTICLE INFO

Article history:
Received 13 June 2010
Received in revised form 9 August 2010
Accepted 10 August 2010
Available online 17 August 2010

Keywords:
Solid oxide fuel cell
Nanostructure
Perovskite
Electrochemical impedance spectroscopy

ABSTRACT

The creation of nanostructured materials with three-dimensional periodicity has been identified as a potential interesting field for increasing the overall performance of solid oxide fuel cells (SOFCs). In this work, we have investigated the formation of $Pr_{0.6}Sr_{0.4}Fe_{0.8}Co_{0.2}O_3$ nanotubes with different diameter sizes employing polymeric membranes as templates. The samples were characterized by X-ray diffraction and field emission scanning electron microscopy. The polarization resistance of the materials was measured by electrochemical impedance spectroscopy (EIS). A study of the influence of the temperature on the nanostructure has also been carried out, demonstrating that the sintering process affects to the electrochemical performance of the cathode. The study shows that the nanotubes with higher diameter size present a better performance at high temperatures than those with diameter sizes smaller than 100 nm. The ASR (area specific resistance) value of the sample synthesized with a pore diameter size of 0.8 μm is as good as 0.12 Ω cm^2, allowing it use as cathode in solid oxide fuel cells (SOFCs).

1. Introduction

Environmental problems are one of the most important challenges for the human future societies. One of the aspects with more influence on this problem is the field of the energy. Several energy devices have appeared and developed in the past decades, fuel cells being one of them. Due to their high efficiency, flexibility with respect to the fuel and low environmental impact, the solid oxide fuel cells (SOFCs) are considered one of the most promising energy conversion devices [1,2]. However, their high operating temperature (800–1000 °C), creates problems associated with the cost of the equipment. This fact has intensified the need of reducing the temperature of the cell to the intermediate range (500–700 °C). Lowering the operation temperature of SOFCs affects not only to the cost, but also to the range of material selection and improves the stability and reliability for the SOFC system [3]. The development of the intermediate temperature solid oxide fuel cells (IT-SOFCs) would promote the introduction of these devices onto the market by reducing manufacturing costs and increasing their durability.

These IT-SOFCs allows the use of new materials such as the nanostructured materials. These new materials are temperature dependent, because the increase of temperature promotes the sintering of the particles changing therefore the structure of the material. The use of nanostructured materials as SOFC electrodes could provide some advantages as the increase of the specific area. This fact is closely related to the creation of double and triple phase boundary (DPB and TPB) which has a great influence in the catalytic activity of the electrodes. Several techniques are being employed in order to obtain new nanostructured materials [4,5]. One of them is the use of polymeric templates as polymethilmetacrilate (PMMA), polystyrene and polycarboxylate. These templates act as pore formers and allow the formation of nanoporous materials [6,7]. Other types of nanostructured materials are the nanotubes, which are commonly obtained employing either polymeric or inorganic membranes.

This paper describes the initial steps in the development of a high performance nanostructured $Pr_{0.6}Sr_{0.4}Fe_{0.8}Co_{0.2}O_3$ material for its application as cathode for SOFCs. The nanostructure includes perovskite-type nanotubes synthesized with polycarbonate porous membranes, with a porous diameter of 0.1 and 0.8 μm.

* Corresponding author at: Department of Inorganic Chemistry, University of the Basque County, Apdo. 644, 48080 Bilbao, Spain. Tel.: +34 94 6012458; fax: +34 94 6013500.
E-mail address: teo.rojo@ehu.es (T. Rojo).

0378-7753/$ – see front matter © 2010 Elsevier B.V. All rights reserved.
doi:10.1016/j.jpowsour.2010.08.015

2. Experimental

2.1. Synthesis of nanostructured $Pr_{0.6}Sr_{0.4}Fe_{0.8}Co_{0.2}O_3$

The $Pr_{0.6}Sr_{0.4}Fe_{0.8}Co_{0.2}O_3$ (PSFC) perovskite-type oxide precursor has been synthesized by the conventional sol–gel method. The sol–gel technique has been particularly investigated because it enables to prepare very fine powders with a low agglomerating degree and for its simplicity to apply this technique in the use of membrane templates [8,9]. Commercial porous polycarbonate membranes (Millipore) with porous diameters of 0.1 and 0.8 μm have been used as template in order to obtain the nanotubes [10]. Metal nitrate salts were used as the starting materials for the final product and citric acid was employed as chelating agent. $Pr(NO_3)_3{\cdot}5H_2O$, $Sr(NO_3)_2$, $Fe(NO_3)_3{\cdot}9H_2O$ and $Co(NO_3)_2{\cdot}6H_2O$ (Sigma Aldrich) were weighted stoichiometrically according to the nominal composition of $Pr_{0.6}Sr_{0.4}Fe_{0.8}Co_{0.2}O_3$ and then dissolved in distilled water. In order to determine the accurate cation stoichiometry of the starting reagents, the corresponding metal nitrates, which are generally hygroscopic, were decomposed up to 1000 °C in a TG/DTA (TA STD 2960). Citric acid was then added into the solution and the resulting mixture was well stirred until it was completely dissolved. After the solution was poured respectively onto the two different polycarbonate membranes (0.1 and 0.8 μm pore diameter size). Once the solution has passed through the membranes, these are removed from the dissolution and a heating process is carried out. The polymer templates were subsequently removed during this thermal treatment at 700 °C in air with a heating rate of 1 °C min^{-1} and also the crystallization of the compounds was reached. Although the crystallization of the compound could be obtained at 600 °C, these extra 100 °C can improve the mechanical resistance of the materials without affecting to the sinterization of the nanostructures [11]. Thus, new materials with a highly ordered three-dimensional nanostructures were obtained.

2.2. X-ray characterization

The X-ray powder diffraction (XRD) data were used to characterize the obtained crystal structure of the as-calcined materials, using a Philips PW1710 diffractometer, with CuK_α radiation and a scanning step 0.02° over the angular range 5°–70°. The obtained data were fitted using the FULLPROF program [12].

2.3. Microstructure analysis

For microstructure analysis, obtained powders were examined by transmission electron microscopy (TEM) using a Philips CM200 transmission electron microscope and by field emission scanning electron microscopy (FESEM) with Schottky emitter using a JEOL JSM-7000F microscope at 20 kV accelerating voltage.

2.4. Electrochemical measurements

Electrochemical impedance spectroscopy (EIS) measurements of symmetrical test cells with samaria doped ceria (SDC) as electrolyte, were conducted using a Solartron 1260 Impedance Analyzer. The frequency range was 10^{-2} to 10^6 Hz with signal amplitude of 50 mV. All these electrochemical experiments were performed at equilibrium from room temperature up to 850 °C and from 850 °C down to room temperature, under both zero dc current intensity and air.

$Ce_{0.8}Sm_{0.2}O_2$ (SDC) has been selected as the electrolyte for the measurements, because of the good performance that it presents at intermediate temperatures [13,14]. The SDC pellets were made using Nextech materials as they were received. The powder of each material was pressed under 5 tons (49,000 N) uniaxial force to form green pellets with a diameter of 1 cm. The pellets were sintered at 1500 °C for 2 h obtaining a density higher than 93% relative to the theoretical value. The surface of the pellets was polished and then cleaned with ethanol and acetone solutions. The area of the pellets was approximately 0.5 cm^2.

In order to prepare the electrodes, the synthesized powders were dispersed in a vehicle ink forming a paste. This paste was painted on both faces of the pellets forming symmetrical cells. These cells were sintered at 1100 °C for 1 h to allow the good adhesion of the cathode on the surface of the electrolytes. As current collector platinum has been used. To ensure the adhesion of the platinum to the cathode surface a thermal treatment at 900 °C was carried out.

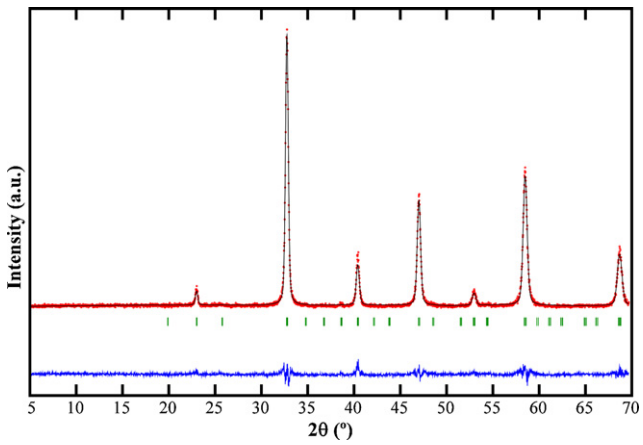

Fig. 1. Diffraction profile of the PSFC phase: experimental (squares), fitted (line) and difference between them (lower line).

3. Results and discussion

3.1. X-ray characterization

$Pr_{0.6}Sr_{0.4}Fe_{0.8}Co_{0.2}O_3$ was obtained as a pure single phase, presenting orthorhombic perovskite structure (space group *Pbnm*), similar to $GdFeO_3$ (see Fig. 1). As the sample prepared with membranes of 0.1 μm (PSFC01) and the prepared with membranes of 0.8 μm (PSFC08) were synthesized from the same dissolution the obtained cell parameters from XRD are similar, being $a = 5.465(6)$ Å, $b = 5.471(3)$ Å and $c = 7.731(6)$ Å.

3.2. Microstructure analysis

The morphology of the synthesized samples can be observed in Fig. 2. The images show nanostructured morphology homogenously distributed along the sample with both polymeric membranes (Fig. 2a and c). Attending to the images with more detail, the perovskite nanotubes and their respective diameters and length can be observed (Fig. 2b and d). Microstructural parameters are given in Table 1, showing that the wall thickness of the prepared tubes is within the nanoscale.

The SEM images in Fig. 2b and c show the perovskite-type hollow nanotubes with diameters of 80 nm for the membranes of the 0.1 μm pore size, and 550 nm for the 0.8 μm membranes (see Table 1). The transmission electron microscopic (TEM) studies on the morphology of the samples synthesized using both templates show the presence of nanotubes of submicron wall thickness (Fig. 3). This hollow morphology is the product of the template assisted synthesis, but this material requires two additional thermal treatments, in order to improve the adhesion of the cathode

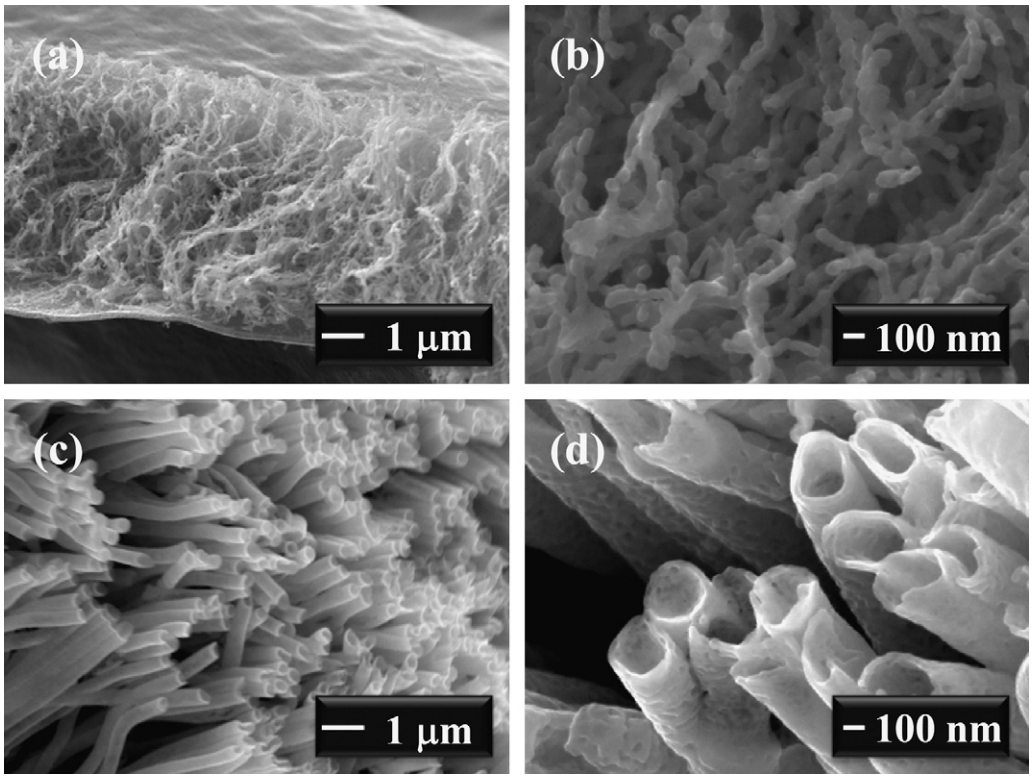

Fig. 2. SEM images of the morphology of the (a and b) PSFC01 and (c and d) PSFC08 nanotubes.

to the electrolyte and also of the platinum ink, which acts as current collector. These thermal treatments need temperatures around 1100 °C, this means that the morphology of the samples can change because of the sintering of the nanotubes. Fig. 4 shows the SEM images of the samples after these two treatments.

The images reveal that the temperature has produced a change in the morphology of both samples. The nanotubes of both samples have suffered a change, turning their tube morphology into thicker nanowires. However the morphology is still three-dimensionally ordered along the sample.

In addition, as the electrochemical measurements are carried out in temperature, another extra thermal treatment is required. Fig. 5 shows the SEM images of the samples after all the treatments that are required including the one that is carried out for the electrochemical measurements of the samples, in other words, Fig. 5 shows the final morphology of the samples.

The SEM images show another change in the morphology of the sample PSFC01. The three-dimension order has disappeared, resulting in a disordered microstructure with a high sinterization degree at some points. Nevertheless the nanotubes of the PSFC08 sample have suffered a smaller change keeping the 3D order and a larger surface area than the sample PSFC01, which facilitates the creation of double phase boundaries (DPBs) in the cathode.

3.3. Electrochemical characterization

The main processes which can take place in the oxygen reduction mechanism on porous MIEC (mixed ionic and electronic conductors) electrodes are the following: (i) diffusion of O_2 molecules in the gas phase to the electrode, (ii) oxygen dissociative adsorption on cathode surface, (iii) surface diffusion of oxygen on the cathode, (iv) incorporation of oxygen into electrolyte via the triple phase boundary (TPB) in the electrode/electrolyte interface, (v) oxide ion incorporation in the bulk of cathode (if mixed conducting), (vi) bulk or surface transport of oxide ion from cathode to electrolyte, and (vii) electrochemical charge transfer across the electrode/electrolyte interface [15–17].

The Nyquist diagrams show the semicircles due to the ionic transport in the electrolyte at low temperatures whereas at high temperatures the phenomena characterizing the cathode/electrolyte/gas interface are found. However, the analysis of EIS plots in terms of fitting with equivalent circuits is complicated because the correlations between the equivalent circuit elements and the actual physical transport and transfer processes at the cathode are vague [18].

The spectra for PSFC/SDC/PSFC cells and their obtained fit measured in air at 700 °C are shown in Fig. 6. R-SDC corresponds to ohmic resistance, R-1 is due to charge transfer and R-2 is attributed

Table 1
Microstructural parameters of the PSFC nanostructures at different temperatures.

Sample	Temperature of the thermal treatment (°C)	Morphology	Wall thickness (nm)	External diameter (nm)	Internal diameter (nm)
PSFC01	600	Nanotubes	20	80	35
	1000 + 900	Nanowires	–	500	–
	850	Disordered microstructure			
PSFC08	600	Nanotubes	100	550	290
	1000 + 900	Nanowires	–	520	–
	850	Nanowires		500–600	

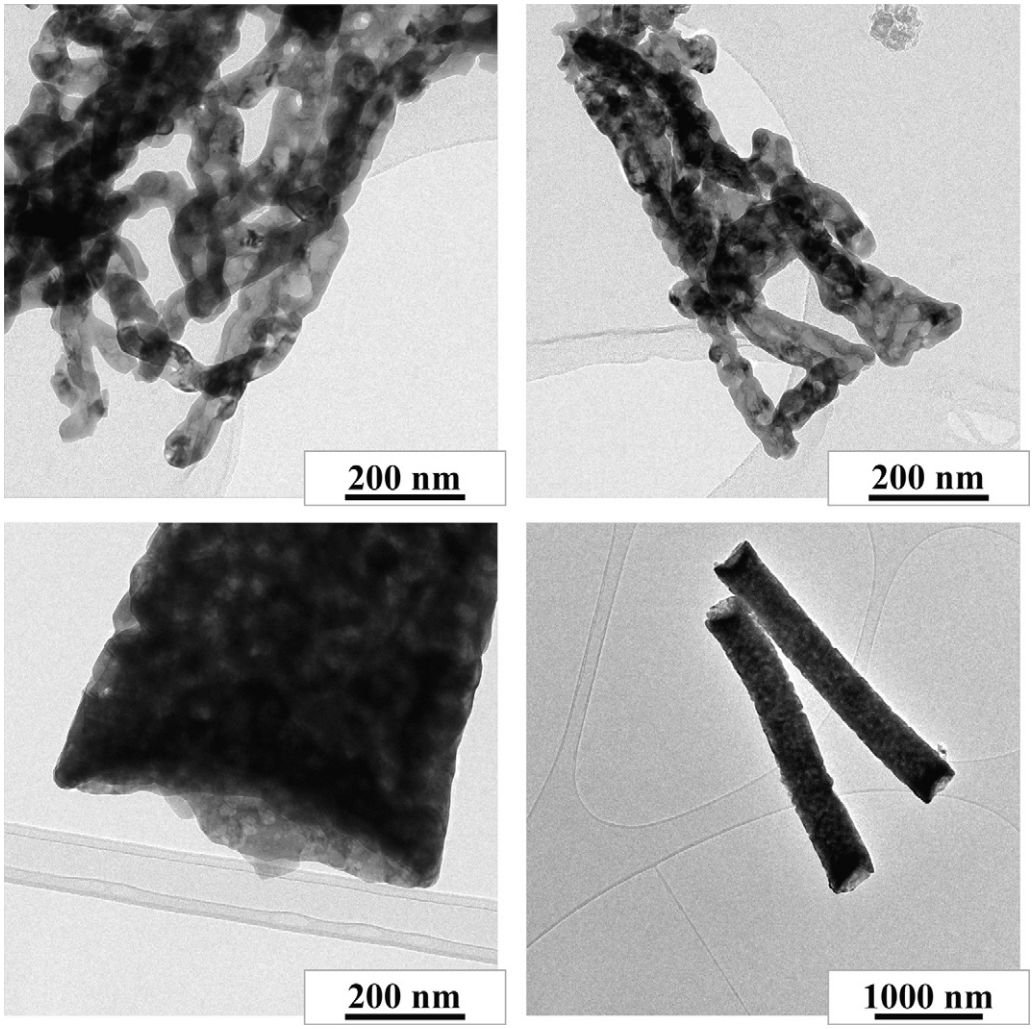

Fig. 3. TEM images of the morphology of the (a) PSFC01 and (b) PSFC08 nanotubes.

to dissociative adsorption on the electrode surface and gas diffusion, respectively [19]. R-1 and R-2 have constant phase elements (CPEs) in parallel to simulate the distribution of relaxation time in the real system. The high-frequency arc (R-1) is assigned to the charge transfer of oxide species across the electrode/electrolyte interface and through the cathode material, followed by the ion incorporation into the electrolyte. This contribution implies a process related to the interface and to the bulk of the cathode, but not to the cathode surface. The contribution of the transport of chemically reduced oxygen through the mixed conductor by solid-state diffusion has been found to be related to the bulk properties of the electrode [20,21]. This way, the oxide ion diffusion in the perovskite-type cathode bulk must be taken into account. Although doped lanthanum cobaltites are widely used as electrode materials for SOFCs due to their mixed ionic–electronic conductivity, when a large amount of Fe is introduced on the Co site, the electronic structure is more complex, exhibiting more semi-conductor-like behavior [22]. As shown by Mizusaki et al. [23], the oxygen non-stoichiometry in orthoferrites is lower than in cobaltites and the oxygen vacancy concentration strongly depends on the oxygen partial pressure. Adler [17] reported that higher electronic conduction is correlated with faster oxygen exchange, while higher vacancy concentration leads to faster ion transport and surface exchange. This way PSFC material tends to have much better surface catalytic properties than more purely ionically conductive materials. Anyway, the oxygen conduction in PSFC perovskite is not negligible. The resistance value corresponding to this high-frequency contribution is similar for the PSFC01 and PSFC08 samples, pointing out that the size and morphology of the nanostructures does not affect the electrode/electrolyte interface. The semicircle of larger size that appears at medium–low frequencies (R-2) is attributed to the surface diffusion ($O^-_{ad} \rightarrow O^-_{TPB}$). The oxide ions formed in the DPB sites must move to the TPB sites to be able to cross the electrolyte. The contribution due to gas diffusion process is usually observed at low frequencies, but at 700 °C this contribution is overlapped with the surface diffusion process and it is difficult to distinguish both contributions. A mechanism of reaction in which the oxygen diminishes chemically on the surface of the mixed conductor exists, followed by the diffusion of the oxygen across the cathode material towards the electrolyte. Diffusion through the porous material is typically described by either ordinary or Knudsen diffusion [24]. As shown in SEM and TEM images, a highly porous material is obtained and in the pores molecules collide more frequently with the pore walls than with other molecules. The mean free path is estimated to be about 68 nm at ambient pressure and taking into account the size of the pores, in PSFC01 gas molecules collide more frequently with the pore walls than with themselves. As a result of frequent collisions with the wall of the pore, the transport of the molecule is impeded [25], facilitating the oxygen adsorption. As shown in Fig. 6, the PSFC01 sample exhibits a lower resistance at

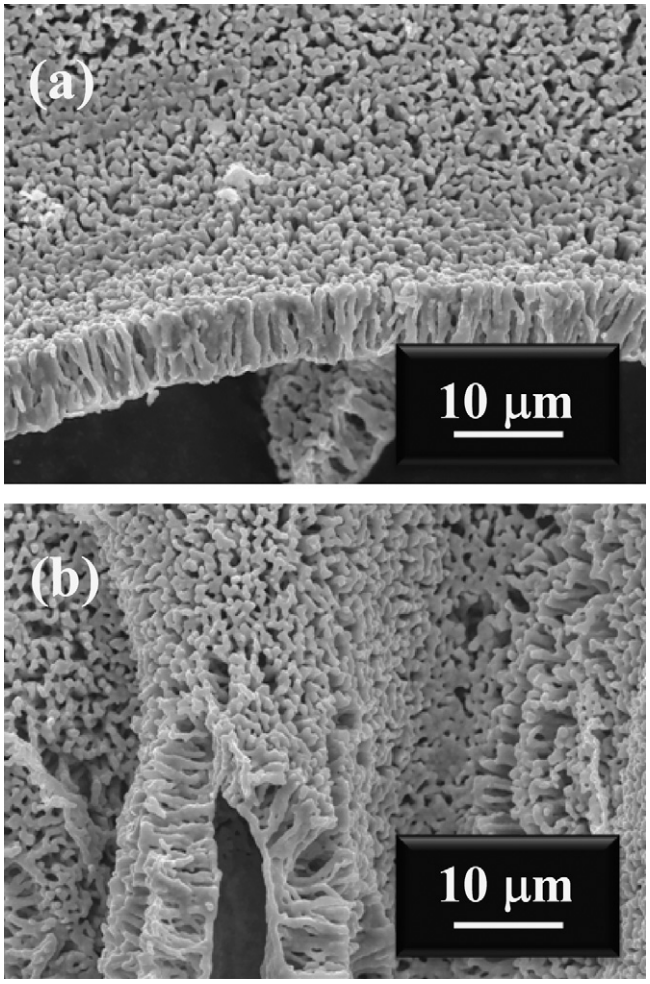

Fig. 4. SEM images after the two thermal treatments required for the adhesion of the cathode and the platinum ink: (a) PSFC01 and (b) PSFC08.

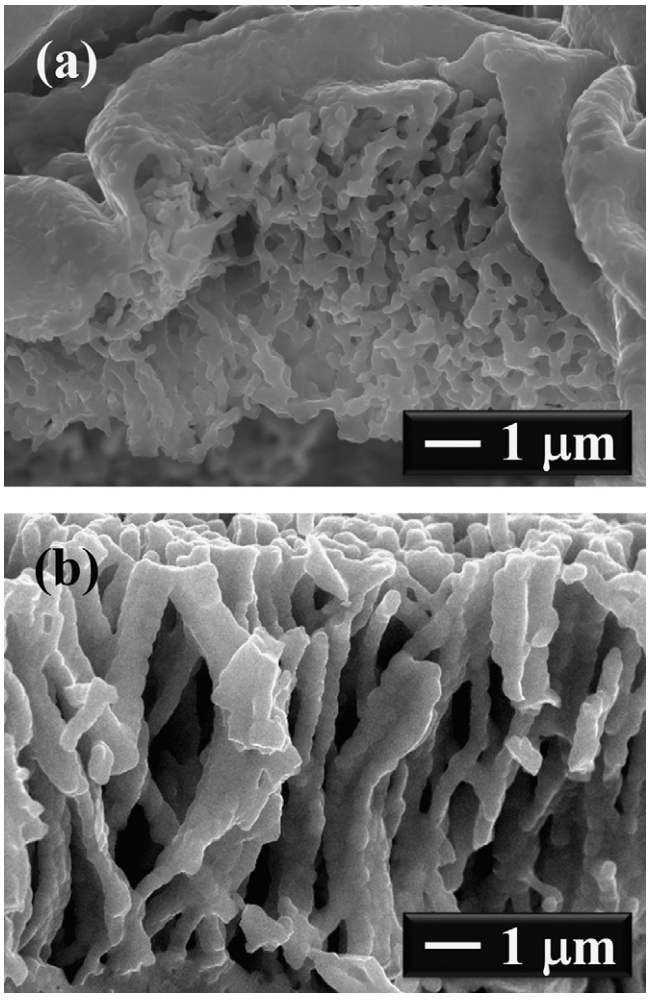

Fig. 5. SEM images of the final morphology of the nanostructured samples: (a) PSFC01 and (b) PSFC08.

700 °C than PSFC08. This fact can be explained due to the smaller size of the nanostructures synthesized with the 0.1 μm pore size membrane. This smaller size could generate more double phase boundaries (DPBs), increasing thereby the active area of the cathode which improves the electrochemical performance of the sample, reducing therefore the semicircle of medium–low frequencies (R-2).

However at 850 °C the PSFC08 sample exhibits a lower resistance than PSFC01, which means that the tendency observed at 700 °C has changed (Fig. 7). A possible explanation for this change can be given taking into account the SEM images of the final morphology of the samples. Fig. 5a shows how the morphology of the sample PSFC01 has suffered a sinterization process, collapsing partially the nanostructure and losing therefore surface area. On the other hand, the PSFC08 sample keeps the desired highly three-dimensional ordered nanostructure after the electrochemical measurement, maintaining also the active zone due to the large surface area, as it can be observed in Fig. 5b. This process was also observed and reported by Sacanell et al. [11] for $La_{0.6}Sr_{0.4}CoO_3$.

Three different semicircles appear at 850 °C. R-SDC, R-1, R-2 and R-3 are related to ohmic resistance, charge transfer and dissociative adsorption on the electrode surface, and gas diffusion, respectively. The appearance of three semicircles at high temperatures is a typical characteristic of the mixed ionic and electronic conductors (MIEC) [26]. The three resistances which belong to the cathode material, R-1, R-2 and R-3, have constant phase elements

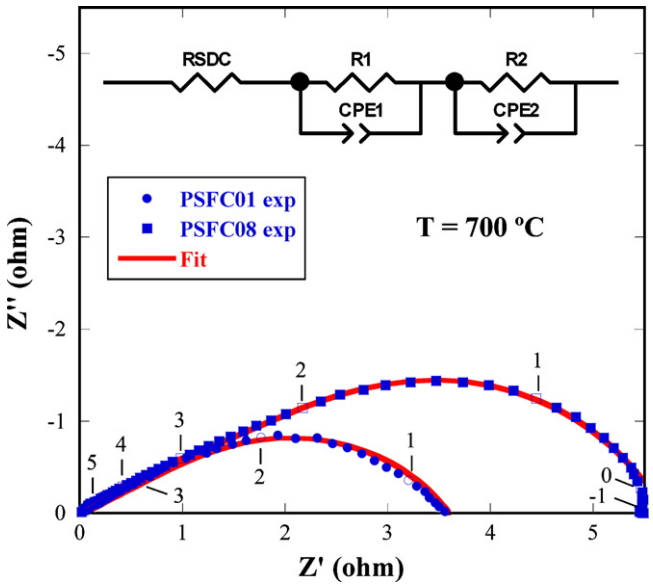

Fig. 6. Nyquist diagram of the PSFC01 and PSFC08 samples at 700 °C. The impedance data are plotted after electrolyte ohmic drop correction. The numbers indicate the frequency logarithm.

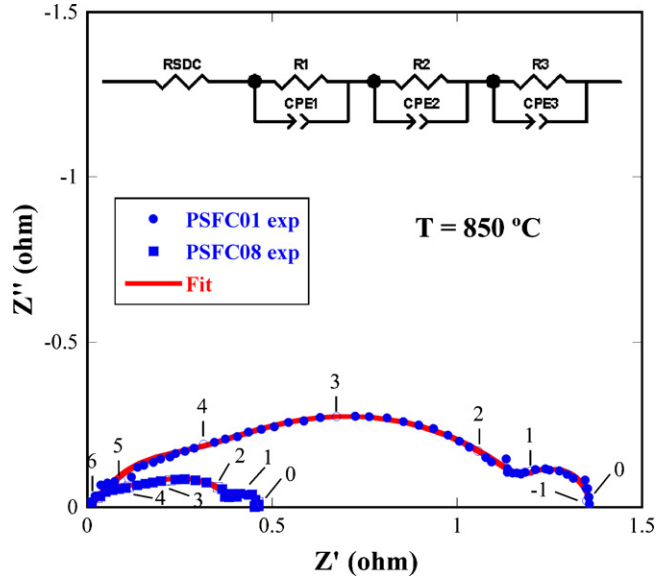

Fig. 7. Nyquist diagram of the PSFC01 and PSFC08 samples at 850 °C. The impedance data are plotted after electrolyte ohmic drop correction. The numbers indicate the frequency logarithm.

(CPEs) in parallel. The overlapping of the semicircles makes difficult the analysis of the results obtained for each process. As it has been mentioned, at both high temperatures and frequencies (R-1), a small arc which is independent of temperature appears [27]. This contribution is similar for both materials, and can be related to the interfacial processes as charge transfer across the electrode/electrolyte interface and solid-state diffusion trough the bulk of the electrode. The medium-frequency arc (R-2) is associated with the processes that take place in the cathodic material, such as oxygen dissociative adsorption on the surface of the electrode and its posterior diffusion towards the electrolyte. These processes are temperature dependent as it can be observed in Figs. 6 and 7. Focusing on the R-2 of both Nyquist diagrams is possible to appreciate the high decrease of this arc when the temperature increases. This considerably decrease observed at 850 °C, allows the appearance of the third semicircle (R-3) which is overlapped at lower temperatures. This low-frequency arc (R-3) is ascribed to the process of gas diffusion, which is highly influenced by the oxygen pressure [28–30]. In order to confirm every contribution with its respective semicircle, it will be necessary to carry out measurements in different oxygen partial pressures, so that study will be carried out in further works under way.

The medium-frequency semicircle is the one which more influence has on the total resistance. For this reason, PSFC08 has a smaller resistance, as the surface area is larger in this sample, the active zone is also larger and therefore there are more sites where the cathodic reaction can takes place, producing a larger amount of oxide ions. On the other hand, the difference in the third semicircle between PSFC01 and PSFC08 can be assigned to the microstructure order. The PSFC08 sample keeps the three-dimension order facilitating the diffusion of the gas through the cathodic material, showing a smaller semicircle than PSFC01 which has lost the microstructural order. Furthermore, the inner pore disappears after the thermal treatments (see Table 1 and Fig. 4) getting nanowires. This way, Knudsen diffusion, when the transport is dominated by collisions with the pore walls, is clearly a dominant process in nanotubes and mesoporous materials.

The EIS data were used to derive the area specific resistance (ASR) for the PSFC electrodes. The cathodic area specific resistance (ASR) is deduced from the relation:

$$\mathrm{ASR} = \frac{R_{\mathrm{electrode}} \times \mathrm{Surface}}{2}$$

The ASR evolution with the temperature for both samples is shown in Fig. 8. The PSFC01 sample presents better ASR values than PSFC08 up to 700 °C. Between 700 and 800 °C the tendency changes showing the PSFC08 a better performance. This change in the tendency can be associated with the loss of the three-dimensional order in the sample PSFC01, while the sample PSFC08 keeps it. At 850 °C the PSFC01 sample exhibits an ASR value of 0.24 Ω cm^2, while the value for the PSFC08 sample is 0.12 Ω cm^2.

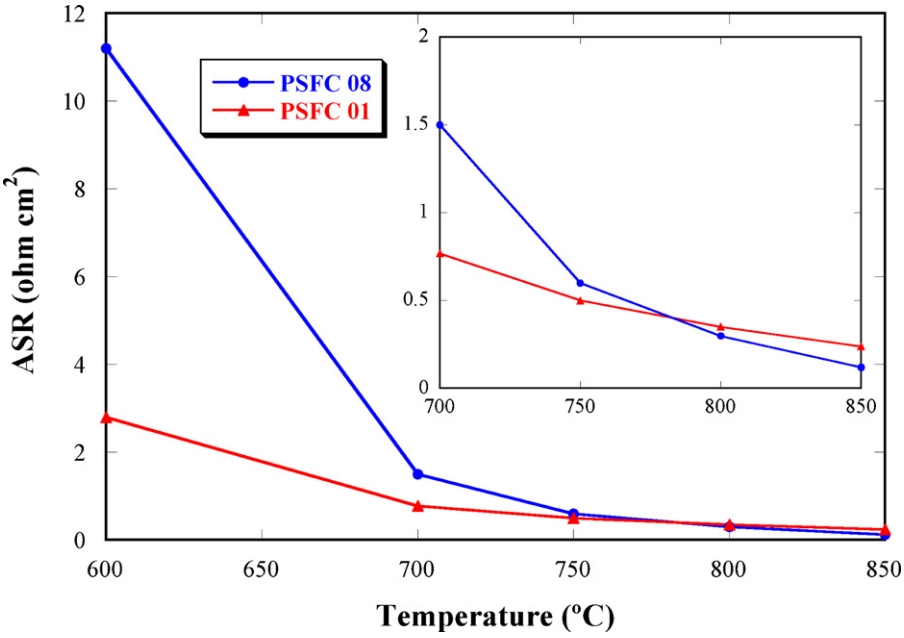

Fig. 8. ASR evolution with temperature of the PSFC01 and PSFC08 samples.

4. Conclusions

3D highly ordered $Pr_{0.6}Sr_{0.4}Fe_{0.8}Co_{0.2}O_3$ nanotubes with different diameter sizes have been synthesized employing commercial polycarbonate membranes. The nanotubes have been characterized by X-ray diffraction proving the presence of an only crystalline phase. A study of the evolution of the morphology with the temperature has been done revealing that the nanotubes with diameter size smaller than 100 nm are more affected by the thermal treatment which derivates in the sintering of the particles, collapsing the nanostructure and reducing the active area of the cathode. On the other hand, the thicker nanotubes are able to keep the nanostructure and that is the reason of their better ASR values at 850 °C, which is as good as 0.12 $\Omega\,cm^2$.

Acknowledgements

This work has been partially financed by the Spanish CiCyT under Project MAT2007-66737-C02-01 and by the Government of the Basque Country under Project IT-312-07. R. Pinedo thanks the University of the Basque Country (UPV/EHU) for his predoctoral fellowship. I. Ruiz de Larramendi thanks the Government of the Basque Country for funding her research activities as postdoc within the Project GIC07/126-IT-312-07. D. Jimenez de Aberasturi thanks the Eusko Jaurlaritza/Gobierno Vasco for her predoctoral fellowship.

References

[1] C. Zhu, X. Liu, D. Xu, D. Wang, D. Yan, L. Pei, J. Power Sources 185 (2008) 212–216.
[2] R. Chiba, H. Orui, T. Komatsu, Y. Tabata, K. Nozawa, M. Arakawa, K. Sato, H. Arai, J. Electrochem. Soc. 155 (6) (2008) B575–B580.
[3] B.C.H. Steele, Nature 400 (1999) 619–621.
[4] W. Ueda, M. Sadakane, H. Ogihara, Catal. Today 132 (2008) 2–8.
[5] S. Woo, K. Dokko, H. Nakano, K. Kanamura, J. Mater. Chem. 18 (2008) 1674–1680.
[6] R. Pinedo, I. Ruiz de Larramendi, J.I. Ruiz de Larramendi, M.I. Arriortua, T. Rojo, Solid State Ionics (2010), doi:10.1016/j.ssi.2010.05.057.
[7] D. Marrero-López, J.C. Ruiz-Morales, J. Peña-Martínez, J. Canales-Vázquez, P. Núñez, J. Solid State Chem. 181 (2008) 685–692.
[8] Z. Yang, Y. Huang, B. Dong, H. Li, Mater. Res. Bull. 41 (2006) 274–281.
[9] N. Ortiz-Vitoriano, I. Ruiz de Larramendi, I. Gil de Muro, J.I. Ruiz de Larramendi, T. Rojo, Mater. Res. Bull. 45 (2010) 1513–1519.
[10] J. Sacanell, M.G. Bellino, D.G. Lamas, A.G. Leyva, Physica B 398 (2007) 341–343.
[11] J. Sacanell, A.G. Leyva, M.G. Bellino, D.G. Lamas, J. Power Sources 195 (2010) 1786–1792.
[12] J. Rodríguez-Carvajal, Physica B 192 (1993) 55.
[13] N. Ortiz-Vitoriano, I. Ruiz de Larramendi, J.I. Ruiz de Larramendi, M.I. Arriortua, T. Rojo, ECS Trans. 25 (2) (2009) 2799–2806.
[14] I. Ruiz de Larramendi, D.G. Lamas, M.D. Cabezas, J.I. Ruiz de Larramendi, N.E. Walsöe de Reca, T. Rojo, J. Power Sources 193 (2009) 774–778.
[15] M. Kleitz, F. Petitbon, Solid State Ionics 92 (1996) 65–74.
[16] A. Ringuedé, J. Fouletier, Solid State Ionics 139 (2001) 167–177.
[17] S.B. Adler, Chem. Rev. 104 (2004) 4791–4843.
[18] E. Magnone, M. Miyayama, E. Traversa, J. Electrochem. Soc. 157 (2010) B357–B364.
[19] M. Koyama, C. Wen, T. Masuyama, J. Otomo, H. Fukunaga, K. Yamada, K. Eguchi, H. Takahashi, J. Electrochem. Soc. 148 (2001) A795–A801.
[20] S.B. Adler, J.A. Lane, B.C.H. Steele, J. Electrochem. Soc. 143 (1996) 3554–3564.
[21] S.B. Adler, Solid State Ionics 111 (1998) 125–134.
[22] T. Ishihara, Perovskite Oxide for Solid Oxide Fuel Cells, first ed., Springer, New York, 2009.
[23] J. Mizusaki, M. Yoshihiro, S. Yamauchi, K. Fueki, J. Solid State Chem. 58 (1985) 257–266.
[24] K. Malek, M.O. Coppens, J. Chem. Phys. 119 (2003) 2801–2811.
[25] C. Berger, Handbook of Fuel Cell Technology, New York, Prentice-Hall, 1968.
[26] F. Mauvy, C. Lalanne, J.M. Bassat, J.C. Grenier, H. Zhao, L. Huo, P. Stevens, J. Electrochem. Soc. 153 (8) (2006) A1547–A1553.
[27] G. Zhu, X. Fang, C. Xia, X. Liu, Ceram. Int. 31 (2005) 115.
[28] D. Perez-Coll, A. Aguadero, M.J. Escudero, P. Nuñez, L. Daza, J. Power Sources 178 (2008) 151–162.
[29] E.P. Murray, T. Tsai, S.A. Barnett, Solid State Ionics 110 (1998) 235–243.
[30] E.P. Murray, S.A. Barnett, Solid State Ionics 143 (2001) 265–273.